Ten- to 50-nm-long quasi-ballistic carbon nanotube devices obtained without complex lithography

Ali Javey, Pengfei Qi, Qian Wang, and Hongjie Dai*

Department of Chemistry and Laboratory of Advanced Materials, Stanford University, Stanford, CA 94305

Edited by Jan D. Achenbach, Northwestern University, Evanston, IL, and approved August 4, 2004 (received for review June 22, 2004)

A simple method combining photolithography and shadow (or angle) evaporation is developed to fabricate single-walled carbon nanotube (SWCNT) devices with tube lengths of ≈10–50 nm between metal contacts. Large numbers of such short devices are obtained without the need of complex tools such as electron beam lithography. Metallic SWCNTs with lengths of ≈10 nm, near the mean free path of $l_{op} \approx 15$ nm for optical phonon scattering, exhibit nearly ballistic transport at high biases and can carry unprecedented 100-μA currents per tube. Semiconducting SWCNT field-effect transistors with ≈50-nm channel lengths are routinely produced to achieve quasi-ballistic operations for molecular transistors. The results demonstrate highly length-scaled and high-performance interconnects and transistors realized with SWCNTs.

Ballistic transport refers to the motion of charge carriers driven by electric fields in a conducting or semiconducting material without scattering. It is a highly desirable phenomenon for a wide range of applications needing high currents, high speeds, and low power dissipations. Single-walled carbon nanotubes (SWCNTs) have been suggested as candidate materials for future electronics, including electrical interconnects and field-effect transistors (FETs) (1–4), for which high current operations are important. It has been shown that among various scattering mechanisms in SWCNTs inelastic optical phonon (OP) scattering/emission has the shortest mean free path (mfp) of $l_{op} \approx 15$ nm, followed by elastic acoustic phonon scattering mfp of $l_{ap} \approx 300$–700 nm at room temperature and defect scattering mfp of $l_e \approx 1$–3 μm (5–8). Transport can be ballistic in relatively long SWCNTs at low bias voltages and electric fields. In the high bias and current regime, however, back scattering of energetic electrons by OP emission causes large channel resistance and limits the current flow, unless the length of the SWCNTs can be reduced $< l_{op} \approx 10$–15 nm (5, 6, 8). There have been several attempts in length scaling of SWCNT devices, and the shortest devices thus far are ≈50 nm long for both metallic (6, 8) and semiconducting SWCNTs (9, 10) fabricated by electron beam lithography. Defining device lengths of <50 nm is difficult by lithographic techniques, although it remains interesting and important to do so to investigate the ultimate current-carrying capability of SWCNTs and push the performance limit of molecular transistors.

Here, we show that by using a simple photolithography and shadow evaporation technique one can readily obtain large numbers of devices comprised of ultrashort SWCNTs down to ≈10 nm between two metal contacts. We found that individual ≈10-nm-long metallic SWCNTs can carry ≈100 μA per tube and are essentially macromolecules with highly ballistic transport properties. By connecting <10 such ultrashort SWCNTs in parallel, one can reach macroscopic current flows on the order of 1 mA. The same fabrication method also affords SWCNT FETs with ≈50-nm channel lengths without relying on electron beam lithography. These highly length-scaled FETs can deliver nearly ballistic currents for transistor operations in the on state.

Methods

We first synthesized SWCNTs by chemical vapor deposition of methane (11) from an array of catalytically patterned sites on Si/SiO_2 substrates (oxide thickness of ≈10 nm in regions that SWCNTs were grown and ≈100 nm in other regions of the substrates). We then formed an array of SWCNT devices, each comprised of two Pd metal contacts (9) spaced at ≈3 μm, by photolithography patterning of resist, metal deposition, and liftoff. The thickness of this first Pd metal deposition varied from $t_1 = 30$ to 50 nm, and sometimes a nominally 0.5-nm-thick Ti was used as an adhesion layer for Pd. The boron-doped Si substrate was used as the gate electrode for the SWCNT devices. Characterization by electrical transport, i.e., conductance vs. gate-voltage (G vs. V_{GS}) and atomic force microscopy (AFM) was used to identify devices with individual metallic or semiconducting SWCNTs bridging the electrode pairs in the array. On a typical 4-by-4-mm chip, tens of individual SWCNT devices were obtained from an array of ≈100.

With these "long" (≈3 μm) SWCNT devices, we carried out a second photolithography step to open windows (≈10 by 10 μm) in a photoresist layer over the SWCNTs and the electrodes and performed angle electron beam evaporation of ≈7-nm-thick Pd followed by liftoff. Because of directional metal deposition of electron beam evaporation, placing the substrate normal at an angle (θ) to the deposition direction afforded shadow formation next to the preformed Pd electrodes. That is, the existing metal electrodes were used as shadow masks for the second metal deposition step to produce small gaps $L \approx t_1 \times tan(\theta) \approx 10$–$50$ nm (for $t_1 = 30$–50 nm and $\theta \approx 20$–$60°$) between source/drain (S/D) electrodes (Fig. 1*a*). SWCNTs bridging these ultrasmall S/D electrodes thus afforded ultrashort tube devices. Fig. 1*b* shows a scanning electron microscopy image of a S/D electrode pair bridged by an $L \approx 15 \pm 5$-nm SWCNT. AFM was also used to characterize these short SWCNT devices. However, for gaps less than ≈30 nm, we found that it is difficult for the AFM tips to reach into the gaps and produce high-quality images.

Results and Discussion

Current saturations are known to occur in long metallic SWCNTs under high bias voltages at the ≈20- to 25-μA level (Fig. 2, tube length $L \approx 1$ μm) due to OP scattering with a short mfp of $l_{op} \approx 10$–15 nm (5, 6, 8). We observed drastically different transport properties for $L \approx 15 \pm 5$-nm metallic SWCNTs (diameter $d \approx 2$ nm), as can be gleaned from the current (I_{DS}) vs. bias voltage (V_{DS}) curve in Fig. 1*c*. In strong contrast to micrometer-long tubes, up to 110 μA of current can be delivered through the ultrashort SWCNT, corresponding to $\approx 4 \times 10^9$ A/cm^2 current density (or 55,000 A/m, normalized by d). This is among the highest current density tolerable by any conductor at room temperature. The ≈100 μA is the highest current transported through a SWCNT, made possible here by forming the shortest and thus most ballistic nanotube channels. In the low bias regime, the I_{DS}–V_{DS} curve is linear with a slope of $G = G_0 T_D T_S$, where $G_0 = 4\ e^2/h$ and $T_S \approx T_D \approx 0.85$ are the transmission probabilities at the source and drain Pd contacts, respectively. At high biases, OP scattering is the dominant

This paper was submitted directly (Track II) to the PNAS office.

Abbreviations: CNT, carbon nanotube; SWCNT, single-walled CNT; mfp, mean free path; FET, field-effect transistor; OP, optical phonon; AFM, atomic force microscopy.

*To whom correspondence should be addressed. E-mail: hdai@stanford.edu.

© 2004 by The National Academy of Sciences of the USA

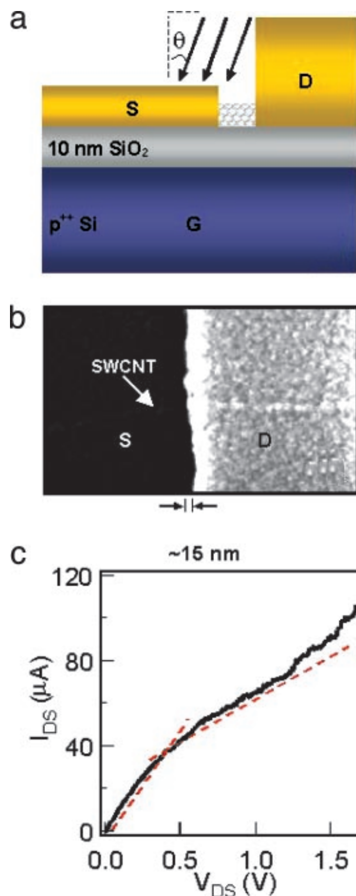

Fig. 1. An ≈10-nm-long metallic nanotube device formed by an angle evaporation method. (*a*) A schematic illustration of the device formation process. A preformed drain (D) electrode is used to mask metal deposition directed at an angle θ with respect to the substrate normal. (*b*) Scanning electron microscopy image of a $L \approx$ 15-nm fabricated SWCNT device. The dark line-like region between the source (S) and D electrodes is ≈15 nm in width and is bridged by a SWCNT. Note that we have not used CNT AFM tips extensively here to characterize the narrow gaps for the following reasons. Multiwalled CNT tips have diameters on the order of 10–30 nm, too large for imaging the narrow gaps. SWCNT tips can be small (down to ≈1 nm in diameter) but are typically short (≈20 nm, for mechanical stiffness) and not suitable for imaging the gaps due to the 30- to 50-nm-tall D electrodes. Our imaging attempts with SWCNT tips encountered the problem of the short tips being incapable of reaching down into the gaps. (*c*) I_{DS}–V_{DS} characteristics of the $L \approx$ 15-nm nanotube ($d \approx$ 2 nm). The lines are drawn to show the slopes of the curve in different bias regimes.

scattering mechanism inside the short nanotube. The transmission probability T caused by OP scattering is related to the nanotube length L and l_{op} by $T = l_{op}/(l_{op} + L)$. The conductance of the nanotube device is $G = \Delta I_{DS}/\Delta V_{DS} = G_0 T_S T_D T$. From the slope of the I_{DS}–V_{DS} curve in the high bias regime and $T_S \approx T_D \approx 0.85$, we obtain $T \approx 0.4$ because of OP scattering. Since $L \approx$ 15 nm as measured by scanning electron microscopy, a transmission probability of $T \approx 0.4$ suggests a mfp of $l_{op} \approx$ 10 nm, which is similar to $l_{op} \approx$ 10–15 nm as measured by independent experiments and groups (5, 6, 8).

Our results show that short SWCNTs are quasi-ballistic macromolecules that can survive high bias voltages and currents. The I_{DS}–V_{DS} curve exhibits an upturn in the slope for biases beyond ≈1.3 V (Fig. 1*c*), attributed to the onset of additional transport through the first noncrossing subband with an energy gap of $\approx 2.6(eV)/d$ (in nm) $\approx 1.3\ eV$ (6). Note that the $\approx 4 \times 10^9$ A/cm^2 current density is 3 orders of magnitude higher than that tolerable by a typical metal before breakdown via electro-migration. CNTs

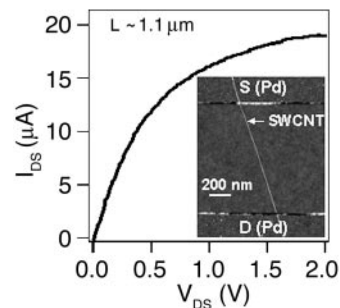

Fig. 2. Current (I_{DS}) vs. bias voltage (V_{DS}) characteristics of an ≈1.1-μm-long SWCNT. The current exhibits saturation under high biases because of scattering by OPs with a short mfp of $l_{op} \approx$ 10–15 nm. (*Inset*) AFM image of the device (SWCNT diameter $d \approx$ 2.5 nm). The line-like structures near the top and bottom of the image correspond to the edges of the source (S) and drain (D) Pd electrodes, respectively. Note that the typical diameters of nanotubes used in the current work are in the range from 1.5 to 3 nm.

can sustain such high currents because of the strong chemical bonding in the covalent sp^2 carbon network. By using the angle evaporation process described above, we have formed eight $L \approx$ 15-nm short devices on an individual SWCNT and then connected them in parallel with comb-like interdigitized electrodes (Fig. 3). Up to 1 mA current can be flowed through such a device (Fig. 3*b*). This finding suggests that if SWCNTs can be close-packed with every tube ohmically contacted, one can afford an ≈1-mA current flow in a region only ≈20 nm wide and ≈2 nm tall. This finding is significant considering that a 50-nm-thick copper film needs to be ≈2 μm wide to carry the same current without breakdown by electromigration. Thus, short CNTs are promising interconnect materials with optimum current-carrying ability, low power dissipation, and superior chemical stability.

With individual semiconducting SWCNTs, we have formed nanotube FETs with $L \approx$ 50-nm channels by using the shadow evaporation technique. Note that the gate dielectric in our current work is ≈10-nm-thick SiO_2 in a back-gate configuration. Although even shorter FETs can be fabricated with our method, we have limited L to approximately >50 nm to avoid short-channel effects. Shown in Fig. 4 is a $L \approx$ 50-nm SWCNT-FET ($d \approx$ 2 nm) with on- and off-current ratio $I_{on}/I_{off} \approx 10^3$ at $V_{DS} = 0.3$ V, a subthreshold swing of ≈300 mV per decade (Fig. 4*b*), and transconductance $(dI_{DS}/dV_G)_{max} \approx 7$ μS. The most notable property of the device is that high current of ≈20 μA can be reached at a low bias voltage of $V_{DS} \approx 0.4$ V (Fig. 4*c*). In comparison, similar currents can be reached only under much higher bias of $V_{DS} \approx 2$ V for $L \approx$ 3-μm SWCNT FETs (9). This finding suggests that the $L \approx$ 50-nm SWCNT FETs are significantly more ballistic than the long channel devices under high bias and current conditions (10). Such transistors are appealing for ultrafast electronics since the on-state current is directly proportional to the speed of a transistor. Further channel length scaling to the $L \approx 5$ nm $< l_{op}$ scale is needed to approach the ultimate ballistic transport limit for CNT-FETs.

In summary, we have obtained large numbers of ultrashort CNT electrical devices without using sophisticated electron beam lithography tools. Our simple shadow evaporation method allows for length scaling of SWCNT electronics down to 10 nm and the elucidation of transport properties at this length scale. Whereas short metallic nanotubes are nearly ballistic conductors useful for future interconnects, short semiconducting nanotubes can be exploited for nearly ballistic transistors for high current operations. In addition, the simple fabrication technique can easily be applied to other materials for obtaining ultraminiaturized devices, including nanowires and nanorods. Thus, highly scaled devices based on chemically derived nanomaterials can now be fabricated in any laboratory with access to simple photolithography tools.

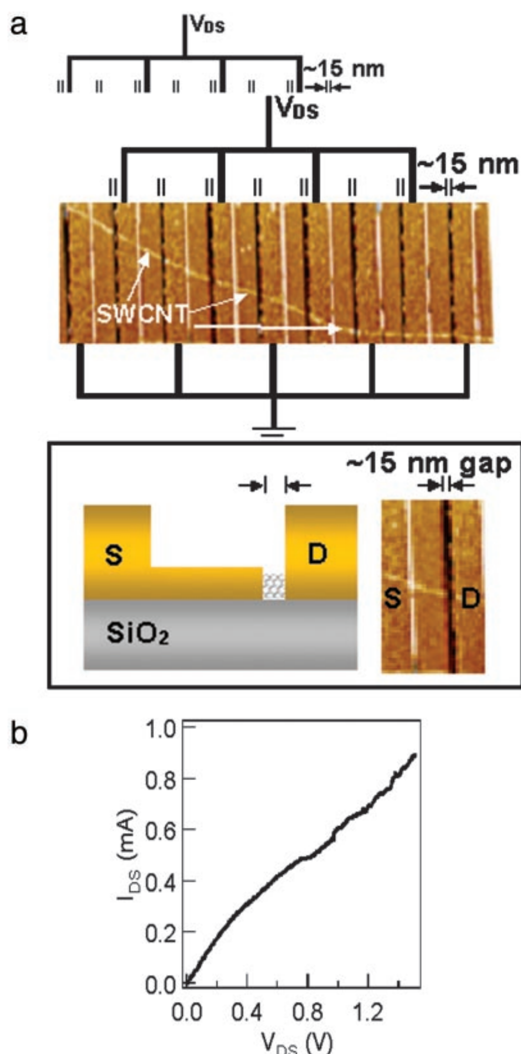

Fig. 3. Eight ultrashort ($L \approx 15$ nm) SWCNTs electrically connected in parallel to carry ≈1-mA current. (*a*) (*Upper*) AFM image of a device comprised of eight short ($L \approx 15$ nm) tube-segments connected in parallel. The eight short-tube devices were formed on a single nanotube ($d \approx 2$ nm) by the following process. A set of parallel metal electrodes (250 nm in width) was first formed on top of the nanotube (electron beam lithography was involved for this experiment). These electrodes were then all used as shadow masks during angle evaporation for the second metal deposition step. Each electrode cast a shadow (dark lines in image) bridged by the nanotube. The multiple shadow devices were then connected in parallel in a comb-like configuration, as drawn. (*Lower*) A schematic side-view structure (*Left*) and top-view AFM image (*Right*) for one of the eight devices. (*b*) I_{DS}–V_{DS} characteristic of the eight tube-devices, showing little current saturation at high biases and a current-carrying capability of ≈1 mA.

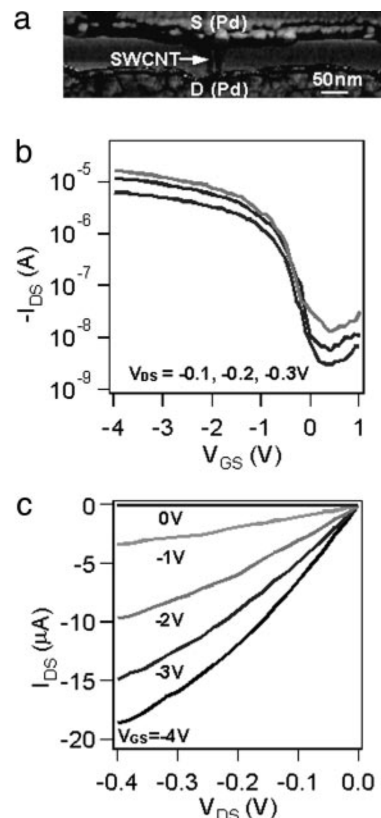

Fig. 4. A $L \approx 50$-nm channel nanotube FET formed by the shadow evaporation method without electron beam lithography. (*a*) AFM tapping-mode phase image of a device with a SWCNT ($d \approx 2$ nm) bridging source (S) and drain (D) electrodes (drain formed by the shadow method). (*b*) I_{DS}–V_{GS} curves recorded at $V_{DS} = -0.1$, -0.2, and -0.3 V. (*c*) I_{DS}–V_{DS} curves recorded at various gate voltages as indicated for the 50-nm SWCNT FET. Specific device fabrication conditions were as follows. The first layer Pd metal thickness was ≈50 nm deposited at 45° to afford a sharp S electrode edge, and the second layer was ≈7 nm of Pd on top of 0.5 nm Ti deposited at a 60° angle. Note that metal deposition by electron beam evaporation is largely directional but diffusive to a small degree. Small numbers of metal atoms may deposit onto the SWCNT in the shadow region, which could then alter the transistor characteristics. We have observed such an effect when attempting channel length scaling down to 10 nm or below. Also note that it is difficult to absolutely ensure that there is a single SWCNT in a device. We used AFM or scanning electron microscopy to ensure that there is only a single connection between the source and drain electrodes. We also often carried out electrical breakdown of the devices at the end of the measurements. Occasional devices exhibiting two current drops (corresponding to breakdown of a two-tube raft or double-walled CNT) are excluded and not presented here.

We thank Marco Rolandi for assistance with an experiment. This work was supported by the Microelectronics Advanced Research Corporation (MARCO) Materials, Structures, and Devices Focus Center, the Stanford Initiative for Nanoscale Materials and Processes, Defense Advanced Research Planning Agency Moletronics, Semiconductor Research Corporation/Advanced Micro Devices, Defense Advanced Research Planning Agency Microsystems Technology Office, a Packard Fellowship, National Science Foundation Network for Computational Nanotechnology, and a Semiconductor Research Corporation Peter Verhofstadt Graduate Fellowship (to A.J.).

1. Dresselhaus, M. S., Dresselhaus, G. & Avouris, P. (2001) *Topics in Applied Physics* (Springer, Berlin), Vol. 80.
2. Dai, H. (2002) *Surf. Sci.* **500,** 218–241.
3. McEuen, P. L., Fuhrer, M. S. & Park, H. K. (2003) *IEEE Trans. Nanotechnol.* **1,** 78–85.
4. Dresselhaus, M. S. & Dai, H., eds. (2004) *MRS Bull. Adv. Carbon Nanotubes* **29,** 237–285.
5. Yao, Z., Kane, C. L. & Dekker, C. (2000) *Phys. Rev. Lett.* **84,** 2941–2944.
6. Javey, A., Guo, J., Paulsson, M., Wang, Q., Mann, D., Lundstrom, M. & Dai, H. (2004) *Phys. Rev. Lett.* **92,** 106804.
7. Mann, D., Javey, A., Kong, J., Wang, Q. & Dai, H. (2003) *Nano Lett.* **3,** 1541–1544.
8. Park, J.-Y., Rosenblatt, S., Yaish, Y., Sazonova, V., Üstünel, H., Braig, S., Arias, T. A., Brouwer, P. W. & McEuen, P. L. (2004) *Nano Lett.* **4,** 517–520.
9. Javey, A., Guo, J., Wang, Q., Lundstrom, M. & Dai, H. J. (2003) *Nature* **424,** 654–657.
10. Javey, A., Guo, J., Farmer, D. B., Wang, Q., Yenilmez, E., Gordon, R. G., Lundstrom, M. & Dai, H. (2004) *Nano Lett.* **4,** 1319–1322.
11. Kong, J., Soh, H., Cassell, A., Quate, C. F. & Dai, H. (1998) *Nature* **395,** 878–881.